ACS APPLIED MATERIALS & INTERFACES

Research Article

www.acsami.org

Photoactive Molecular Junctions Based on Self-Assembled Monolayers of Indoline Dyes

Lorenzo Caranzi,[†,‡] Giuseppina Pace,[†] Simone Guarnera,[†,‡] Eleonora V. Canesi,[†] Luigi Brambilla,[§] Sai S. K. Raavi,[†,#] Annamaria Petrozza,[†] and Mario Caironi*[,†]

[†]Center for Nano Science and Technology @PoliMi, Istituto Italiano di Tecnologia, Via Pascoli 70/3, 20133 Milano, Italy

[‡]Dipartimento di Fisica, Politecnico di Milano, Piazza Leonardo da Vinci 32, 20133 Milano, Italy

[§]Dipartimento di Chimica, Materiali e Ingegneria Chimica "Natta", Politecnico di Milano, Piazza Leonardo da Vinci 32, 20133 Milano, Italy

Supporting Information

ABSTRACT: We demonstrate the feasibility of a photodetector based on an ensemble molecular junction, where a self-assembled monolayer of an organic donor−acceptor dye is directly sandwiched between two electrodes. In such a device, upon photoexcitation and generation of a charge-transfer state on the molecule, charges are dissociated and directly collected at the electrodes without the need of transport through a bulk phase, as in usual photodetectors. We show that the device can work in photovoltaic regime and the spectral response can be tuned by varying the light absorbing dye. Therefore, the electro-optical properties of the downscaled device can be unambiguously related to the physical−chemical properties of the molecules, a commonly difficult point to demonstrate in a molecular junction device, because of the uncertainties of the interplay between molecules and electrodes. The proposed device, which relies on a simple self-assembly process, has a strong potentiality for fast responding, downscaled detectors, ultimately limited by charge dissociation dynamics, and can be considered also as a useful tool to investigate fundamental electro-optical processes in molecular monolayers.

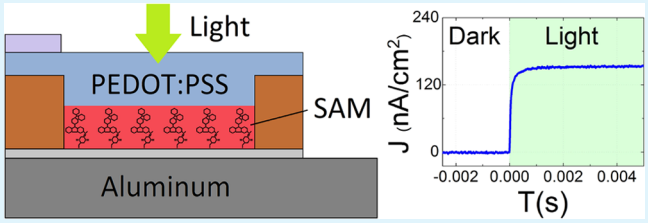

KEYWORDS: *molecular electronics, self-assembled monolayers, molecular junctions, photodetectors, organic dyes*

INTRODUCTION

Since the first theoretical prediction of molecular rectifiers,[1] the field of molecular electronics has been extensively explored, with the aim of studying and controlling charge transport through single molecules. Nevertheless, the difficulty of relating the electrical behavior of a molecular junction to the physical and chemical properties of the molecule itself still represents one of the main issues to be faced. Thanks to their unique properties, such as their easy-processing and thermodynamic stability, self-assembled monolayers (SAMs) have been widely used to fabricate ensemble molecular junctions.[2−6] Unlike junctions based on the scanning probe microscopy techniques or break junctions,[7−9] ensemble junctions consist in a large number of molecules packed between two electrodes. These junctions have allowed the study of different kind of molecules, from simple alkyl chains,[10−12] to conjugated molecules.[13,14] While saturated carbon chains provide a good test-bed for molecular junctions architectures, favoring the assessment of their reliability by studying molecular dependent tunneling currents, conjugated molecules enable the development of functional junctions, that is, junctions which can provide an optoelectronic functionality and may therefore be adopted in future molecular circuits and/or sensors. The growing interest for optically responsive organic devices, like molecular and polymeric photodetectors, led to a special focus on photosensitive molecules. Molecular junction based optoelectronic switches have been demonstrated,[15,16] together with optically responsive molecular memories,[17] and SAMs photosensitized metal/oxide electrodes.[18,19] Photocurrent generation from SAMs is shown in photoelectrochemical cells.[20−24] However, there exists little work on solid state devices based on photoresponsive monolayers.[25,26]

Here we demonstrate the possibility of fabricating a solid state light sensitive molecular junction that allows the measurement of a photocurrent generated by the light absorption of a molecular monolayer. In 1980, Kuhn et al.[27,28] showed the photocurrent extraction from a sandwich structure composed of alternate layers of donor and acceptor molecules. The molecular photodetector proposed here is instead based on a single active layer composed by donor−acceptor (D−A) molecules, which present an intramolecular charge transfer (ICT) excited state. These molecules are widely used in dye-sensitized solar cells (DSSCs),[29] since they induce charge separation and injection in electron transporting media,

Received: July 26, 2014
Accepted: November 3, 2014
Published: November 3, 2014

such as TiO_2 and ZnO, giving rise to the photovoltaic effect. The creation of the ICT as well as the charge injection in the metal-oxide semiconductor are generally fast processes, that is, fs–ps time scales,[30−32] depending on the chosen dye, on its electronic structure and on the metal oxide accepting states. Such ultrafast charge injection time-scales can be exploited for achieving high frequency responses in organic molecule based photodetectors, where no charge transport is involved.

The structure of our device is characterized by a simple architecture that can be integrated with conventional electronics, thanks to the easy-processing of the self-assembly. After optimization of the self-assembling process and the verification of the presence of a monolayer, the active layer is simply sandwiched between two electrodes. Upon photoexcitation, owing to its strong intramolecular charge transfer nature, the locally excited state quickly evolves into an ICT state with lower binding energy enabling easy charge-dissociation. The charges are directly extracted by the contacts allowing the flow of photocurrent. The flowing direction of the photocurrent is imposed by the position of the D–A groups relative to the electrodes and, importantly, the spectral photoresponse can be unambiguously related to the chemical and physical properties of the organic molecule, thus allowing a molecular tuning of the spectral selectivity. In order to fully exploit the potential offered by the proposed molecular detector, we optimized the structure of the device, focusing in particular on the enhancement of the photoresponse, critically limited by extrinsic factors which are strongly related to the choice of the electrodes, and on the improvement of the dynamic response. Such a molecular junction can be considered both a fundamental research tool for directly investigating the optoelectronics properties of molecular ensambles in simplified structures and a potential platform for the development of a fast photodetector, thus facilitating the integration of downscaled photodetecting elements in complex electronic systems (e.g., lab-on-chips).

EXPERIMENTAL METHODS

Device Preparation. A 60 nm aluminum bottom contact was thermally evaporated on a Corning 1737F glass substrate. The detectors active area was defined by a conventional photolithographic process employing S1813 as photoresist, deposited by spin-coating onto the aluminum bottom electrode at 5000 r.p.m. for 1 min to form a 1 μm thick layer, subsequently exposed to a mercury UV lamp through a photomask. After development, the photoresist layer was hard-baked at 150 °C for 2 h in a nitrogen glovebox. For the samples with plasma grown native oxide, the aluminum was exposed for 10 min to 100 W oxygen plasma. The molecular SAM was grown on the exposed aluminum areas by immersion of the substrates in a solution (0.4 mM) of acetonitrile/tert-butanol (50%vol) for 2 h. The substrates were then rinsed, immersed for 5 min in clean acetonitrile and then strongly shaken in order to remove the physisorbed molecules lying onto the SAM. After the substrate was rinsed a second time in acetonitrile, PEDOT:PSS was spin-coated at 4000 r.p.m. for 1 min. Two different PEDOT:PSS formulations have been used, a high conductivity one, referred as HC-PDT (Agfa Orgacon ICP 1050 showing 0.1 Ω cm) and a low conductivity one, referred as LC-PDT (Heraeus Clevios AI 4083 showing 2000 Ω cm). To obtain a complete desorption of water from the PEDOT:PSS layer, the device was baked at 120 °C for 30 min. Finally, a silver paste drop was deposited next to the active area to facilitate the electric contact between the probes tips and the PEDOT:PSS top electrode.

Infrared Measurements. Absorbance spectra of the dyes in powder samples have been recorded with a Nicolet FT-IR Nexus spectrometer coupled to a Thermo Electron Continuμm Microscope using a Diamond Anvil Cell (DAC). Reflection absorption infrared spectroscopy (RAIRS) spectra of SAM samples prepared on naturally oxidized aluminum sputtered glass substrate have been recorded at grazing angle incidence with a Thermo Fisher Nicolet FTIR 6700 spectrometer equipped with a liquid N_2 cooled MCTA detector using a Spectra-Tech FT-80 Grazing Angle accessory and P polarized IR beam. Both IR absorption and RAIRS spectra have been recorded with a resolution of 4 cm^{-1}.

Optoelectronic Measurements. All the time dependent photocurrent and current density/voltage measurements were acquired with a B1500A Semiconductor device parameter analyzer provided by Agilent Technologies. Devices were illuminated by various LEDs covering the spectrum range between 370 and 710 nm. EQE measurements were performed in high-vacuum condition (10^{-5} mbar), while dynamics and *JV* characteristics were obtained in a controlled nitrogen atmosphere.

TA Measurements. The femtosecond transient absorption measurements are based on an amplified mode locked Ti:sapphire laser (Clark-MXR Model CPA-1), delivering pulses at 1 kHz repetition rate with 780 nm center wavelength, 150 fs duration. In the present experiment, we used two pump pulses centered at 390 and 530 nm, respectively. The 390 nm pulses are obtained directly by the second harmonic of 780 nm making use of suitable cut BBO crystal. To obtain 530 nm we employed the noncollinear optical parametric amplifier (NOPA) setup capable of delivering tunable pulses in the visible (500–700 nm) with ∼10 nm bandwidth. A small fraction of the Ti:sapphire amplified output is focused into a 2 mm-thick sapphire plate to generate a stable single-filament white-light supercontinuum, which serves as a probe pulse, spanning from 400 to 1000 nm. The pump and probe beams are spatially and temporally overlapped on the sample, controlling the time delay by motorized slit. The minimum detectable signal is $\Delta T/T \approx 10^{-4}$. The system has a ∼150 fs temporal resolution. The pump beam density energy used in the experiment is kept deliberately low (50 nJ energy, 300 μm beam size). All the measurements were taken with the samples in a vacuum chamber, to prevent any influence from oxygen or sample degradation.

RESULTS AND DISCUSSION

Materials and Layout of the Device. Fabrication of monolayer-based photodetectors requires the active layer to be composed of strong light-absorbing molecules, which can show easy photoinduced charge separation. We investigated the donor–acceptor organic dyes D102, D131, and D205, the chemical structure of which is showed in Figure 1. These dyes have high molar extinction coefficient in the visible region of the spectrum and are widely adopted as efficient sensitizers in DSSCs.[33−35] They are characterized by a conjugated donor indoline-based group where the HOMO electron density is mainly found. The acceptor moiety, where the LUMO charge density is mostly localized, varies across the three dyes. The HOMO energetic level is similar for all the dyes (around −5.4 eV), while the LUMO level varies, being −2.35 eV for D131, −2.59 eV for D102, and −2.66 eV for D205, thus leading to different energy gaps and optical absorption spectral ranges.[36] A carboxylic group chemically linked to the acceptor is present, and it enables the binding to various metal oxide surfaces.

The device structure of our photodiode is shown in Figure 2, and it is based on the high yield, large area molecular junction proposed by Akkerman et al. in 2002,[37,38] resulting in a vertical structure photodetector.

An aluminum bottom electrode has been thermally evaporated onto a glass substrate. The aluminum surface naturally oxidizes upon exposure to air, creating a thin layer of native aluminum oxide, therefore favoring the chemisorption of the molecule thanks to its anchoring carboxylic group. Subsequently, a photoresist layer has been deposited on the

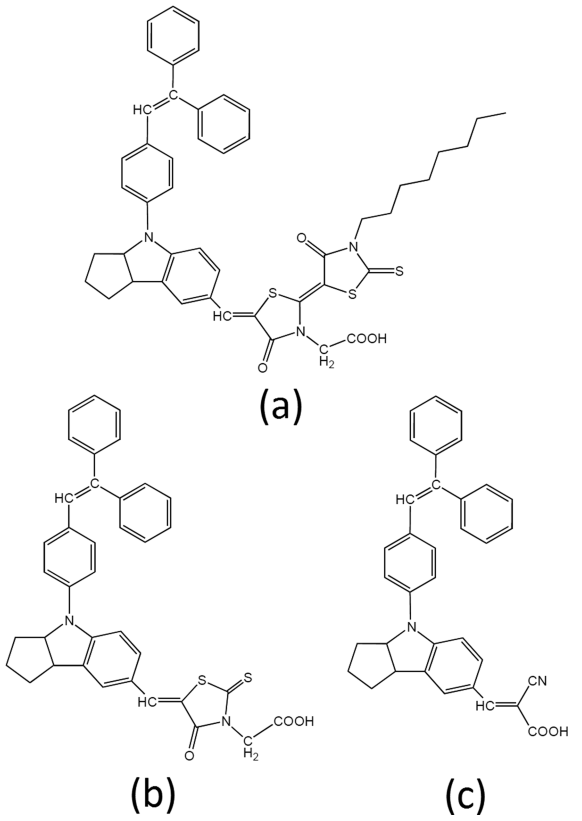

Figure 1. Molecular structure of the indoline based dyes used as active layer in the photodetector: (a) D205, (b) D102, and (c) D131.

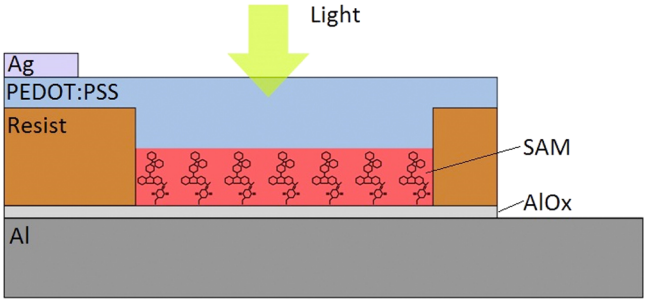

Figure 2. Schematic cross section of the molecular junction based photodetector. Incident light passes through the transparent PEDOT:PSS top electrode and reaches the active monolayer (highlighted in red) which is grown on the thin native AlO_x layer on top of the Al electrode.

aluminum by spin-coating. Part of the photoresist was then removed by means of a photolithographic process, leading to holes of 1 mm^2 corresponding to the active area of the device. The SAM was grown directly onto the exposed native aluminum oxide of the active area by immersion in the dye solution.[39] Once the SAM was formed, a poly(3,4-ethylenedioxythiophene) poly(styrenesulfonate) (PEDOT:PSS) top contact was spin-coated directly onto the SAM. The PEDOT:PSS thin layer is a transparent and conductive top electrode, allowing both light transmission and charge collection.

SAMs Characterization. The formation of a chemisorbed SAM is very critical as it is at the base of the proposed molecular detector. The self-assembling procedure was therefore optimized, as described in the Experimental Methods, and carefully characterized to verify the presence of a single molecular layer. Three different experimental techniques were adopted: reflection absorption infrared spectroscopy (RAIRS) on freshly deposited molecular layers in order to verify the anchoring and to exclude the presence of multiple physisorbed layers; UV−vis absorption measurements of desorbed molecules in order to estimate the surface coverage; AFM measurements before and after the dyes deposition to characterize the surface roughness and further exclude the presence of large aggregates. While RAIRS is a direct method to obtain information about the presence of a chemical bond to the substrate, UV−vis and AFM measurements provide an indirect proof of the absence of aggregates, which could give rise to bulk photogeneration. The extrapolation of SAM packing on the surface is beyond the scope of the current analysis.

In Figure 3a, we reported the IR absorption spectrum of the D131 powder sample and the RAIRS spectrum of the SAM of

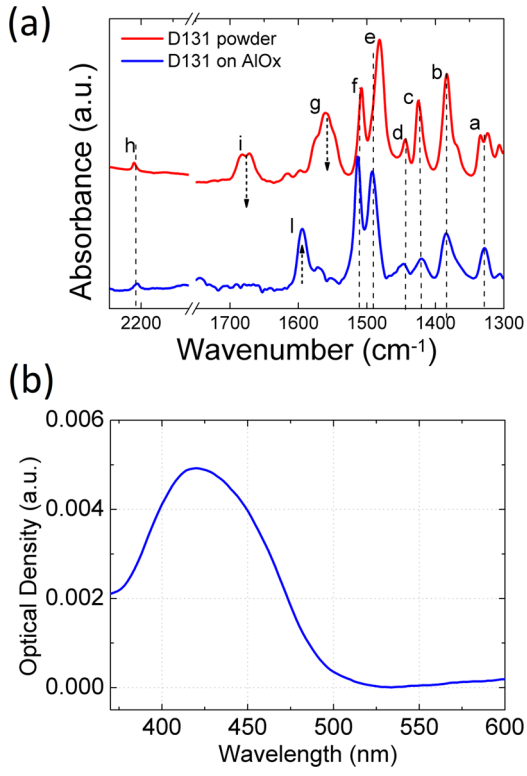

Figure 3. (a) Transmission IR spectrum of D131 in powder (red line) and RAIRS of the D131 monolayer (blue line). (b) Optical density of the D131 molecules desorbed from the aluminum contact and dissolved in a solution of NaOH diluted in water.

D131 on aluminum oxide. The D131 was chosen among the other molecules because it is characterized by the simplest molecular structure of the anchoring functionality. In particular, the presence of only one carbonyl group allows for a straightforward assignment of the C═O stretching vibration as a signature of the SAM formation. Since the purpose of the study is to focus on the SAM formation, we discuss here the main IR bands that prove the presence and the binding of the dyes. In the absorption spectrum of powder D131 (see Figure 3a) we identify a set of medium/strong bands: (a) a doublet with component at 1324 and 1334 cm^{-1}, (b) a band at 1380, (c) at 1424, (d) at 1443, (e) at 1481, and (f) at 1508 cm^{-1}, and

dx.doi.org/10.1021/am5049465 | ACS Appl. Mater. Interfaces 2014, 6, 19774−19782

(g) a broad and structured feature with maximum at 1560 cm^{-1}. These bands form a spectral pattern common to all the samples (see Supporting Information, Figure S1) and can be associated with the vibrations of the common mojety of the three dyes. Band (i) is a doublet, with components at 1683 and 1671 cm^{-1}, and it is assigned to the C═O stretching vibration of the carboxylic group, likely involved in the formation of dimers through hydrogen bonds.[40] Band (h) at 2223 cm^{-1} is assigned to the nitrile group (−CN) stretching vibration. In the RAIRS spectrum of D131 bands from a to f and band h appear similar with respect to those of the absorption spectrum of the powder. Bands e and f show different relative intensities and are blue-shifted, while band h is red-shifted. This matching of signals confirms the presence of D131 on the surface. Bands g and i (C═O stretching) disappear in the RAIRS, while a new band (l) appears at 1590 cm^{-1}, which is assigned to the antisymmetric stretching of the carboxylate group ($-COO^-$).[41] This proves the occurrence of a bidentate/chelating bond between the molecule and the AlO_x substrate through the $-COO^-$ groups.[42,43] Since the band (i) of the carboxylic group is not present in the SAM spectrum, any substantial presence of physisorbed D131 molecules can be excluded. Consistent results have been obtained with dyes D102 and D205 (see Supporting Information, SI, Figure S1).

To quantitatively investigate the presence of a monolayer, we performed a coverage estimation through UV−vis absorption. A SAM was grown on a wide aluminum thin film of a known area. The monolayer was then desorbed in a diluted NaOH solution in water and collected in a cuvette. The UV−vis absorption spectrum obtained from this solution is shown in Figure 3b. The shape of the spectrum traces the one of the molecule in solution, with the characteristic absorption peak at 425 nm. Knowing the molar extinction coefficient at 416 nm, the measured optical density and taking into account the mean surface roughness (measured with AFM, see Supporting Information, Figure S3), we found a surface density of $C = 5.26 \times 10^{13}$ molecules cm^{-2}, comparable with literature values found for the binding to a TiO_2 substrate.[44]Following the same procedure we obtained the coverage values for the other dyes that result to be 2.50×10^{13} and 1.65×10^{13} molecules cm^{-2} respectively for D102 and D205 (see Supporting Information). The resulting mean molecular areas are 1.90 (D131), 4.00 (D102), and 6.06 nm^2 (D205). These coverage values are only slightly lower than the ones reported in the literature, possibly due to the presence of defects in the monolayer.[44] These molecular areas are also in apparent agreement with the D205 and D102 being oriented parallel to the surface, and D131 standing vertically, as suggested by literature.[44] The absence of large aggregates is confirmed by AFM measurements of the aluminum surface. AFM measurements show no differences on the topography of the aluminum contact before and after the monolayer deposition (see Supporting Information Figure S3). Importantly, this is consistent with both RAIRS and coverage evidence and it reasonably excludes the substantial presence of physisorbed molecular aggregates.

Optoelectronic Characterization. Figure 4a shows the current density versus voltage (*JV*) characteristics of a molecular junction photodetector based on D205 in dark and light conditions (505 nm excitation wavelength, light-emitting diode, LED, source, 11 mW cm^{-2}). The dark current is symmetric, showing low current densities and reaching 100 nA cm^{-2} when the device is biased at 0.5 V. The *JV* curve under light conditions demonstrates the generation of a photocurrent,

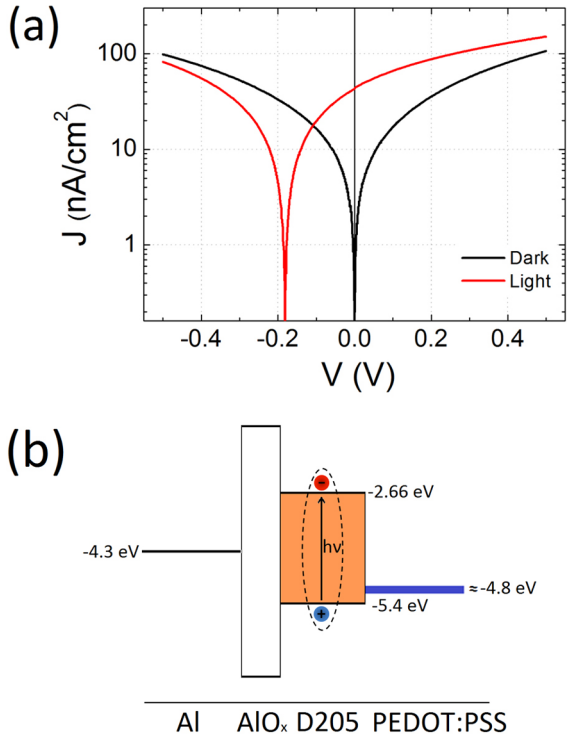

Figure 4. Optoelectronic characterization of a photodetector obtained with a D205 monolayer. (a) *JV* curves under dark (black line) and light (red line) conditions under 505 nm LED illumination (11 mW cm^{-2}); a positive bias refers to the application of a positive voltage to the Al with respect to PEDOT:PSS electrode. (b) A simplified energy levels diagram of a photoexcited device biased in short circuit conditions.

with an open circuit voltage (V_{OC}) of 180 mV and a short circuit current density (J_{SC}) of 43 nA cm^{-2}. This is remarkable for a monolayer based device and convincingly demonstrates the feasibility of a molecular junction photodetector, capable of operating in a photovoltaic regime. In short-circuit conditions, upon absorption of a photon, a charge transfer state is formed leading to the photogeneration of separated charges with electrons flowing to the aluminum bottom electrode, and holes to the PEDOT:PSS. According to the energy level scheme of Figure 4b, the application of a positive bias to the aluminum bottom electrode with respect to the top electrode facilitates the collection of the photoexcited charges in the direction favored by the CT state, that is, collection of electrons at the bottom electrode and of holes at the PEDOT:PSS one. Similar *JV* curves have been measured also for the other dyes (D131, D102) (see Supporting Information Figure S4). Devices based on D102 and D131 showed lower V_{OC} (140 and 130 mV, respectively) and comparable photocurrents (47 and 38 nA cm^{-2}). We observed that the measured value for the V_{OC} is not related to the type of dye used, but rather to the slope of the dark *JV*, and thus to the resistance value of the junction: this indicates that since the V_{OC} is strongly correlated to the shunt resistance, likely originating from defects in the SAM where the PEDOT:PSS and aluminum oxide are in direct contact, it is this parameter which is sizing the V_{OC} in our large area diode.

These results indicate that electrons are capable to overcome the potential barrier of the thin aluminum oxide even in short circuit conditions. On the other hand, the application of a negative bias to the aluminum electrode with respect to the PEDOT:PSS is reflected in a force which drives the charges in

an opposite direction compared to the one favored by the charge transfer state, thus resulting in a smaller amount of photocurrent.

EQE spectra, taken in photovoltaic conditions (0 V), are presented in Figure 5 and are compared with the absorption

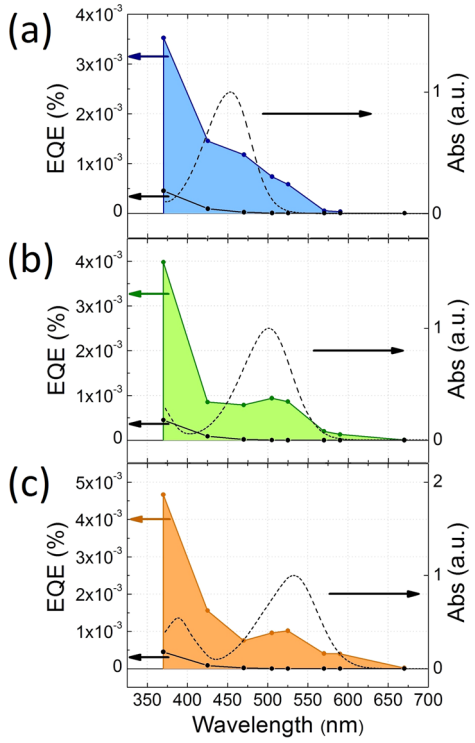

Figure 5. EQE spectra of the molecular junction based photodetectors fabricated with the different indoline based dyes: (a) D131, (b) D102, and (c) D205. Black solid line refers to the spectral contribution of a device containing only a PEDOT:PSS layer and AlO_x interface, in absence of the monolayer. Normalized absorption spectra of dyes in solution are shown with a dashed black line.

spectra of the dyes in solution. The three dyes show comparable EQE values, consistently with their similar molar extinction coefficients (around 50000−55000 M^{-1} cm^{-1}) and SAM surface density. Focusing on the spectral features, we can recognize a strong photoresponse in the near UV region and a relative maximum in the visible spectral range whose position depends on the dye used, that is, at 425, 505 and 525 nm for D131, D102, and D205, respectively. The black solid line in Figure 5a−c is associated with the photoresponse of a device fabricated without the molecular monolayer, containing only a PEDOT:PSS layer. This reference device shows only a weak photocurrent at 370 nm, indicating that the interface between PEDOT:PSS and the native oxide cannot generate any photocurrent in the visible region while it weakly contributes to the UV response. Comparable EQE were also obtained with further control devices made with a non photoactive SAM of saturated carbon chains (see related discussion in Supporting Information, Figure S8). The measured photocurrent in the monolayer based devices can be therefore attributed without any ambiguity to the self-assembled molecules, demonstrating the possibility to tune the spectral response of molecular junctions based photodetectors.

The EQE values measured at the absorption peak of each dye are 1.45 × 10^{-3}% for D131, 0.87 × 10^{-3}% for D102, and 0.94 × 10^{-3}%. This is in agreement with the fact that the optical density of the monolayer of D131, scaling with the product between the coverage value and the molar extinction coefficient, is higher than the one found for the other dyes. Such a low EQE is reasonable, if we consider the reduced optical density of the monolayer resulting in a very small fraction of light absorbed. We estimated the percentage of light absorbed to be around 0.4−1% of the incident light. Such magnitude of the absorption allows a first order estimation of the Internal Quantum Efficiency of 0.1−0.2%, depending on the considered dye. Therefore, despite the proximity of the electrodes, collection is not efficient, suggesting the presence of a limiting mechanism.

To clarify the working mechanism of this device we performed further fundamental investigations. First, femtosecond transient absorption (TA) measurements were run on D205 sensitized mesoporous alumina and mesoporous titania. Mesoporous oxides enabled achieving an optical density high enough to be compatible with the technique sensitivity. Mesoporous titania is a well-established electron acceptor and we used it as a control sample for charge injection from the photoexcited dye. Differential transmission ($\Delta T/T$) spectra upon photoexcitation at 530 nm are shown in Supporting Information Figure S5. In the spectral range between 450 and 600 nm, a positive band can be observed, which we assign to the molecule photobleaching (PB). In Figure 6, the kinetics probed at 480 nm are shown for the case of the molecule deposited on the Al_2O_3 and on the TiO_2 substrate. In the first case, the $\Delta T/T$ signal remains positive, simply monitoring the full recover of the molecule ground state. When the D205 sensitizes the TiO_2, the $\Delta T/T$ signal changes its sign, indicating the formation of a photoinduced absorption (PA) band. We

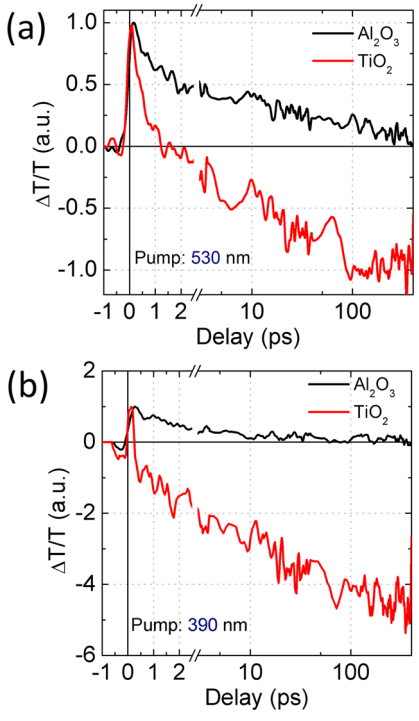

Figure 6. Transient absorption measurement of mesoporous Al_2O_3 and TiO_2 substrates sensitized with D205, probed at 480 nm and pumped with laser light at 530 (a) and 390 nm (b). The black dashed line at zero delay indicates the time of pump pulse, data are normalized at the maximum of the signal.

dx.doi.org/10.1021/am5049465 | ACS Appl. Mater. Interfaces 2014, 6, 19774−19782

assign it to the absorption of $D205^+$ species created upon electrons injection from the dye to the TiO_2. This confirms that there is no charge separation at the $D205/Al_2O_3$ interface and consequently indicates that the presence of the Al native oxide in our device may represent a barrier for the electron extraction and a source of loss.

Despite this higher barrier for electron transfer, in our devices a detectable photocurrent can be recorded. There are two possible explanations for this: on the one hand electrons can have a relatively high probability to tunnel through the thin, noncompact native oxide;[45] on the other, since the native oxide is nonstoichiometric, we cannot exclude that charge collection could be also mediated by the presence of intragap trap states, where electrons may be transferred, to be subsequently released to the conducting states of the underlying conductive aluminum layer. The role of the bottom interface can be evidenced on devices with an aluminum oxide grown by oxygen plasma: the measured photocurrent is strongly reduced when the oxide is treated with plasma (see Supporting Information Figure S6), confirming the importance of the nature of aluminum oxide for the charge transfer from the molecule to the bottom electrode. While demonstrating that the thin native oxide does not hamper electrons collection, we are also gathering indications about a possible limit of the present architecture.

Besides the combined role of molecules and bottom interface in sizing the quantum efficiency, we also observed that the amount of dark current is not influenced by the choice of the dye or by the oxide treatment, indicating that the high resistivity of this low conductive PEDOT:PSS layer is strongly limiting the dark current (see Figure S9–S10 and related discussion in Supporting Information). The role of the PEDOT:PSS on the dark currents was then examined in depth, comparing devices made with differently conductive PEDOT:PSS formulations (PDT): a low conductivity (0.0005 S cm^{-1}) and a high conductivity (10 S cm^{-1}) one, indicated as LC-PDT and HC-PDT in the following, respectively. The magnitude of the photocurrent generated by the two devices is similar, indicating that the photogeneration mechanism is independent of the PDT contact. On the other hand, the strong variation in the dark current (see Supporting Information Figure S9) suggests that the resistance of the junction is scaling with the conductivity of the PDT used. Nonetheless, the use of HC-PDT is not sufficient to highlight the effect of the SAM in the dark currents, since there is no substantial variation between the devices made with and without the SAM. Although PEDOT:PSS is significantly influencing the dark currents, it has to be underlined that our highest values of dark current densities, obtained with HC-PDT, are 6 orders of magnitude lower than the literature values for Au/SAM/PEDOT:PSS junctions,[37] indicating that in the devices with HC-PDT the aluminum oxide is the most resistive element in the junction.

The top contact conductivity can also influence the junction response time upon illumination, which is an important aspect for a photodetecting device. Indeed the relatively low conductivity of the contacting polymer, combined with the high capacitance of the junction, may produce large time constants and therefore represent a possible limiting factor. Considering the equivalent circuit of the device, the whole impedance of the circuit can be simplified as a series between the resistance of the PDT (R_S) and dye/AlOx/Al ensemble, composed by the capacitance C of the junction in parallel with its resistance R_P. R_S can be seen as the sum of a vertical R_V and a lateral R_L contribution, affected by the anisotropic conductivity of a PDT thin film.[46] The dynamic behavior of the device is thus limited by the RC time constant τ_{RC} given by the junction capacitance (C) and the parallel between R_S and R_P (R, see Supporting Information eq S2). Figure 7a shows the

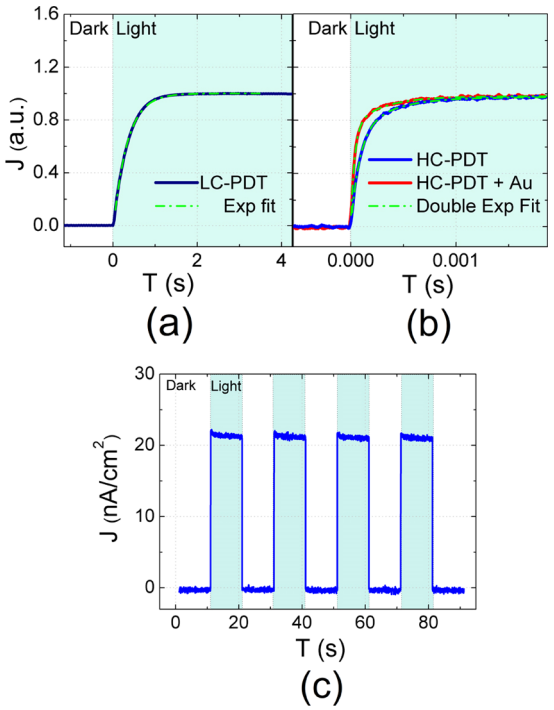

Figure 7. Photocurrent time response for D205 photodetector (incident wavelength 425 nm). (a) Devices based on LC-PDT, (b) devices based on HC-PDT (blue solid line) and with HC-PDT covered with a semitransparent gold electrode (red solid line), and (c) Photocurrent time response measured for a photodetector based on HC-PDT in alternated dark/light conditions and 505 nm incident light.

dynamic response of the device made with the LC-PDT at 0 V bias applied. The transient photocurrent is perfectly fitted with a single exponential, demonstrating that a single RC of the device is actually limiting the dynamic behavior. The time constant τ is very large, around 330 ms. In this case, the resistance values are measured to be 200 MΩ and 250 MΩ for R_S and R_P, respectively (see Figures S11, S12, and impedance discussion in Supporting Information), caused by the chosen LC-PDT. The capacitance value of the junction can be correspondingly derived to be approximately 3 nF.

In Figure 7b, the dynamic response of a device based on the 4 orders of magnitude more conductive HC-PDT is shown (blue solid line). In this case, the rising edge is at least 3 orders of magnitude faster, showing two different time constant contributions: a dominating one (τ_1) of 100 μs and a slower and less significant contribution (τ_2) of 650 μs. For this device we measured much lower R_S and R_P values, of 5 kΩ and 710 kΩ, respectively. The dynamic response of the device is thus limited by the lowest value given by R_S. Knowing in this case both the value of C (7.7 nF) and R_S (see Figure S11, S12, and related discussion in Supporting Information), we can therefore estimate the limiting τ_{RC}, which turns out to be 40 μs. This means that the increased conductivity of the PDT has actually improved the dynamic response of the device, mostly because of the lowering of the series resistance of the device itself.

dx.doi.org/10.1021/am5049465 | ACS Appl. Mater. Interfaces 2014, 6, 19774–19782

In order to further reduce the HC-PDT total resistance by lowering its lateral resistance, we evaporated a semitransparent layer of gold (10 nm) on top of the PDT electrode. The semitransparent gold layer strongly reduces the lateral resistance R_L of the entire top-contact, allowing us to further decrease R_S down to 25 Ω while maintaining a capacitance value of 7.7 nF (see Supporting Information Figure S12). In Figure 7b, the dynamics obtained are reported (red solid line). The gold top contact enables the fastest rise edge given by our devices. The time response shows a dominating τ_1 of 35 μs and a slower and a less influential τ_2 of 338 μs, while the calculated time constant τ_{RC} is 0.2 μs. Despite the 2 orders of magnitude change of the R_S resistance, we observe only a reduction of a factor 3 in the measured response time, implying that other mechanisms are limiting the dynamic response in this device. Possibly a trap assisted injection mechanism at the AlO_x or SAM/PDT interface could be responsible for this limitation. We speculate that dyes with different anchoring group could be adopted in order to overcome the limit of the metal oxide interlayer and to foster a faster injection.

Finally, in Figure 7c the photoresponse of a molecular junction photodetector made with HC-PDT and top gold electrode to a train of light pulses can be appreciated. This behavior is highly reproducible, the device is stable and it remains functional for months if kept in a nitrogen controlled atmosphere, displaying two of the essential features of a functional photodetector.

CONCLUSIONS

We have demonstrated the possibility to fabricate a molecular junction based photodetector by sandwiching a SAM of indoline dyes between two electrodes. The bottom contact is an aluminum electrode with a native oxide where the carboxylic acid group of the molecules binds, and the top electrode is a polymer conductor. The photogeneration mechanism unambiguously involves the molecular monolayer, as testified by the possibility to tune the photoresponse spectrum by adopting dyes with different energy gaps. Electro-optical characterizations show that the devices can work in photovoltaic regime with all the investigated dyes (D102, D131, D205), benefiting of large ratios between dark and photocurrents close to short-circuit conditions, a promising aspect toward highly sensitive molecular photodetectors. In particular, we have recorded a maximum V_{OC} value of 180 mV with dye D205 and a maximum J_{SC} of 47 nA/cm^2 with dye D102. The dark current is clearly influenced and limited by the interfaces and electrodes. The dynamic response upon photoexcitation is influenced by the nature of the electrodes as well and can be strongly improved by lowering the resistance of the top contact made of PEDOT:PSS. When a semitransparent Au electrode is deposited on top of the polymer conductor a minimum time constant of 35 μs could be achieved. Considering the development of nanostructured photodetectors, this molecular junction not only paves the way for the implementation of promising photosensitive devices, fabricated via simple self-assembling processes, but it is also a valuable instrument to carry out fundamental studies on the charge photogeneration, separation, and collection at the interface between molecular monolayers and electrodes, still requiring a deeper comprehension. The key aspect is the demonstrated possibility to disentangle physical-chemical molecular properties from the optoelectronic response of a solid-state, photosensitive molecular junction.

ASSOCIATED CONTENT

Supporting Information

RAIRS of D102 and D205 monolayers, absorption of the desorbed D102 and D205 in solution, AFM measurements of the substrates, *JV* curves for D131 and D205 devices, transient absorption spectra of the mesoporous titania and alumina sensitized with D205, photocurrent of devices made with D102, dark *JV* characteristics of native and plasma grown oxide based devices, with and without D102 SAM, molecular structure, *JV* characteristics in dark and under light conditions and EQE of devices made with a SAM of tridecanoic acid, *JV* curves of devices with and without D205 with different top electrodes, mean values and standard deviations of the *JV* characteristics of several devices made with the low and high conductive PEDOT:PSS, equivalent circuit of the devices and corresponding frequency dependence of the impedance, frequency dependence of D205 devices with different top contact, and impedance values and time constants related to three devices based on different top electrodes. This material is available free of charge via the Internet at http://pubs.acs.org.

AUTHOR INFORMATION

Corresponding Author

*E-mail: mario.caironi@iit.it.

Present Address

[#]Sai S. K. Raavi: Department of Physics, Indian Institute of Technology Hyderabad, Yeddumailaram 502205, Telengana, India.

Author Contributions

The manuscript was written through contributions of all authors. All authors have given approval to the final version of the manuscript.

Funding

It is acknowledged the financial support from Fondazione Cariplo under project Indixi, Grant no. 2011-0368. M.C. acknowledges financial support from European Union through the Marie-Curie Career Integration Grant 2011 "IPPIA", within the European Union Seventh Framework Programme (FP7/2007-2013) under grant agreement PCIG09-GA-2011-291844.

Notes

The authors declare no competing financial interest.

ACKNOWLEDGMENTS

The authors acknowledge the kind support and help of D. Natali, F. Maddalena, A. Iacchetti, M. Binda, A. Grimoldi, and A. R. Srimath Kandada with the data interpretation of impedance measurements, EQE measurements and transient absorption measurements. It is acknowledged the financial support from Fondazione Cariplo under project Indixi, Grant no. 2011-0368. M. C. acknowledges financial support from European Union through the Marie-Curie Career Integration Grant 2011 "IPPIA", within the European Union Seventh Framework Programme (FP7/2007-2013) under grant agreement PCIG09-GA-2011-291844.

REFERENCES

(1) Aviram, A.; Ratner, M. A. Molecular Rectifier. *Chem. Phys. Lett.* **1975**, *29*, 277−283.

(2) Zhou, C.; Deshpande, M. R.; Reed, M. A.; Jones, L., II; Tour, J. M. Nanoscale Metal/Self-Assembled Monolayer/Metal Heterostructures. *Appl. Phys. Lett.* **1997**, *71*, 611−613.

(3) Chen, X.; Jeon, Y.-M.; Jang, J.-W.; Qin, L.; Huo, F.; Wei, W.; Mirkin, C. A. On-Wire Lithography-Generated Molecule-Based Transport Junctions: A New Testbed for Molecular Electronics. *J. Am. Chem. Soc.* **2008**, *130*, 8166−8168.
(4) Cai, L. T.; Skulason, H.; Kushmerick, J. G.; Pollack, S. K.; Naciri, J.; Shashidhar, R.; Allara, D. L.; Mallouk, T. E.; Mayer, T. S. Nanowire-Based Molecular Monolayer Junctions: Synthesis, Assembly, and Electrical Characterization. *J. Phys. Chem. B* **2004**, *108*, 2827−2832.
(5) McCreery, R. L.; Wu, J.; Kalakodimi, R. P. Electron Transport and Redox Reactions in Carbon-Based Molecular Electronic Junctions. *Phys. Chem. Chem. Phys.* **2006**, *8*, 2572−2590.
(6) Grave, C.; Tran, E.; Samorì, P.; Whitesides, G. M.; Rampi, M. A. Correlating Electrical Properties and Molecular Structure of SAMs Organized Between Two Metal Surfaces. *Synth. Met.* **2004**, *147*, 11−18.
(7) Bumm, L. A.; Arnold, J. J.; Cygan, M. T.; Dunbar, T. D.; Burgin, T. P.; Jones, L., II; Allara, D. L.; Tour, J. M.; Weiss, P. S. Are Single Molecular Wires Conducting? *Science* **1996**, *271* (5256), 1705−1707.
(8) Wold, D. J.; Frisbie, C. D. Fabrication and Characterization of Metal−Molecule−Metal Junctions by Conducting Probe Atomic Force Microscopy. *J. Am. Chem. Soc.* **2001**, *123*, 5549−5556.
(9) Elbing, M.; Ochs, R.; Koentopp, M.; Fischer, M.; Von Hänisch, C.; Weigend, F.; Evers, F.; Weber, H. B.; Mayor, M. A Single-Molecule Diode. *Proc. Natl. Acad. Sci. U.S.A.* **2005**, *102*, 8815−8820.
(10) Slowinski, K.; Chamberlain, R. V.; Miller, C. J.; Majda, M. Through-Bond and Chain-to-Chain Coupling. Two Pathways in Electron Tunneling Through Liquid Alkanethiol Monolayers on Mercury Electrodes. *J. Am. Chem. Soc.* **1997**, *119*, 11910−11919.
(11) Wang, W.; Lee, T.; Reed, M. A. Mechanism of Electron Conduction in Self-Assembled Alkanethiol Monolayer Devices. *Phys. Rev. B* **2003**, *68*, 035416,1−7.
(12) Wang, G.; Kim, Y.; Choe, M.; Kim, T. W.; Lee, T. A New Approach for Molecular Electronic Junctions with a Multilayer Graphene Electrode. *Adv. Mater.* **2011**, *23*, 755−760.
(13) Chen, J.; Reed, M. A.; Rawlett, A. M.; Tour, J. M. Large On−Off Ratios and Negative Differential Resistance in a Molecular Electronic Device. *Science* **1999**, *286*, 1550−1551.
(14) Wang, G.; Kim, T. W.; Jang, Y. H.; Lee, T. Effects of Metal−Molecule Contact and Molecular Structure on Molecular Electronic Conduction in Nonresonant Tunneling Regime: Alkyl versus Conjugated Molecules. *J. Phys. Chem. C* **2008**, *112*, 13010−13016.
(15) Kronemeijer, A. J.; Akkerman, H. B.; Kudernac, T.; van Wees, B. J.; Feringa, B. L.; Blom, P. W. M.; de Boer, B. Reversible Conductance Switching in Molecular Devices. *Adv. Mater.* **2008**, *20*, 1467−1473.
(16) Li, T.; Jevric, M.; Hauptmann, J. R.; Hviid, R.; Wei, Z.; Wang, R.; Reeler, N. E. A.; Thyrhaug, E.; Petersen, S.; Meyer, J. A. S.; Bovet, N.; Vosch, T.; Nygård, J.; Qiu, X.; Hu, W.; Liu, Y.; Solomon, G. C.; Kjaergaard, H. G.; Bjørnholm, T.; Brøndsted Nielsen, M.; Laursen, B. W.; Nørgaard, K. Ultrathin Reduced Graphene Oxide Films as Transparent Top-Contacts for Light Switchable Solid-State Molecular Junctions. *Adv. Mater.* **2013**, *25*, 4164−4170.
(17) Simao, C.; Mas-Torrent, M.; Crivillers, N.; Lloveras, V.; Artés, J. M.; Gorostiza, P.; Veciana, J.; Rovira, C. A Robust Molecular Platform for Non-Volatile Memory Devices with Optical and Magnetic Responses. *Nat. Chem.* **2011**, *3*, 359−364.
(18) Furmansky, Y.; Sasson, H.; Liddell, P.; Gust, D.; Ashkenasyd, N.; Visoly-Fisher, I. Porphyrins as ITO Photosensitizers: Substituents Control Photo-Induced Electron Transfer Direction. *J. Mater. Chem.* **2012**, *22*, 20334−20341.
(19) Gao, L.; Sun, Q.; Wang, K. Photoelectrochemical Properties of a Series of Electrostatically Self-Assembled Films Based on Sandwich-Type Polyoxometalates and a Bichromophore Hemicyanine Dye. *J. Colloid Interface Sci.* **2013**, *393*, 92−96.
(20) Matsuo, Y.; Lacher, S.; Sakamoto, A.; Matsuo, K.; Nakamura, E. Conical Pentaaryl[60]fullerene Thiols: Self-Assembled Monolayers on Gold and Photocurrent Generating Property. *J. Phys. Chem. C* **2010**, *114*, 17741−17752.
(21) Gatto, E.; Caruso, M.; Porchetta, A.; Toniolo, C.; Formaggio, F.; Crisma, M.; Venanzi, M. Photocurrent Generation Through Peptide-Based Self-Assembled Monolayers on a Gold Surface: Antenna and Junction Effects. *J. Pept. Sci.* **2011**, *17*, 124−131.
(22) Vijayaraghavan, R. K.; Gholamrezaie, F.; Meskers, S. C. J. Photovoltaic Effect in Self-Assembled Molecular Monolayers on Gold: Influence of Orbital Energy Level Alignment on Short-Circuit Current Generation. *J. Phys. Chem. C* **2013**, *117*, 16820−16829.
(23) Imahori, H.; Norieda, H.; Yamada, H.; Nishimura, Y.; Yamazaki, I.; Sakata, Y.; Fukuzumi, S. Light-Harvesting and Photocurrent Generation by Gold Electrodes Modified with Mixed Self-Assembled Monolayers of Boron−Dipyrrin and Ferrocene−Porphyrin−Fullerene Triad. *J. Am. Chem. Soc.* **2001**, *123*, 100−110.
(24) Imahori, H.; Kimura, M.; Hosomizu, K.; Sato, T.; Ahn, T. K.; Kim, S. K.; Kim, D.; Nishimura, Y.; Yamazaki, I.; Araki, Y.; Ito, O.; Fukuzumi, S. Vectorial Electron Relay at ITO Electrodes Modified with Self-Assembled Monolayers of Ferrocene−Porphyrin−Fullerene Triads and Porphyrin−Fullerene Dyads for Molecular Photovoltaic Devices. *Chem.—Eur. J.* **2004**, *10*, 5111−5122.
(25) Burtman, V.; Zelichonok, A.; Pakoulek, A. V. Molecular Photovoltaics in Nanoscale Dimension. *Int. J. Mol. Sci.* **2011**, *12*, 173−225.
(26) Xia, F.; Mueller, T.; Lin, Y.; Valdes-Garcia, A.; Avouris, P. Ultrafast Graphene Photodetector. *Nat. Nanotechnol.* **2009**, *4*, 839−843.
(27) Polymeropoulos, E. E.; Möbius, D.; Kuhn, H. Monolayer Assemblies with Functional Units of Sensitizing and Conducting Molecular Components: Photovoltage, Dark Conduction and Photoconduction in Systems with Aluminium and Barium Electrodes. *Thin Solid Films* **1980**, *68*, 173−190.
(28) Fujihira, M.; Nishiyama, K.; Yamada, H. Photoelectrochemical Responses of Optically Transparent Electrodes Modified with Langmuir−Blodgett Films Consisting of Surfactant Derivatives of Electron Donor, Acceptor and Sensitizer Molecules. *Thin Solid Fims* **1985**, *132*, 77−82.
(29) O'Regan, B.; Grätzel, M. A Low-Cost, High-Efficiency Solar Cell Based on Dye-Sensitized Colloidal TiO_2 Films. *Nature* **1991**, *353*, 737−740.
(30) Cheng, H.-M.; Hsieh, W.-F. Electron Transfer Properties of Organic Dye-Sensitized Solar Cells Based on Indoline Sensitizers with ZnO Nanoparticles. *Nanotechnology* **2010**, *21*, 485202.
(31) Sai Santosh Kumar, R.; Grancini, G.; Petrozza, A.; Abrusci, A.; Snaith, H. J.; Lanzani, G. Effect of Polymer Morphology on P3HT-Based Solid-State Dye Sensitized Solar Cells: an ultrafast Spectroscopic Investigation. *Opt. Express* **2013**, *21*, A469−A474.
(32) Abrusci, A.; Sai Santosh Kumar, R.; Al-Hashimi, M.; Heeney, M.; Petrozza, A.; Snaith, H. J. Influence of Ion Induced Local Coulomb Field and Polarity on Charge Generation and Efficiency in Poly(3-Hexylthiophene)-Based Solid-State Dye-Sensitized Solar Cells. *Adv. Fun. Mater.* **2011**, *21*, 2571−2579.
(33) Schmidt-Mende, L.; Bach, U.; Humphry-Baker, R.; Horiuci, T.; Miura, H.; Ito, S.; Uchida, S.; Gratzel, M. Organic Dye for Highly Efficient Solid-State Dye-Sensitized Solar Cells. *Adv. Mater.* **2005**, *17*, 813.
(34) Huang, L. H.; Jiang, L. L.; Wei, M. D. Metal-Free Indoline Dye Sensitized Solar Cells Based on Nanocrystalline Zn_2SnO_4. *Electrochem. Commun.* **2010**, *12*, 319−322.
(35) Ito, S.; Miura, H.; Uchida, S.; Takata, M.; Sumiok, K.; Liska, P.; Comte, P.; Péchy, P.; Grätzel, M. High-Conversion-Efficiency Organic Dye-Sensitized Solar Cells with a Novel Indoline Dye. *Chem. Commun.* **2008**, 5194−5196.
(36) Le Bahers, T.; Pauporte, T.; Scalmani, G.; Adamo, C.; Ciofini, I. A TD-DFT Investigation of Ground and Excited State Properties in Indoline Dyes Used for Dye-Sensitized Solar Cells. *Phys. Chem. Chem. Phys.* **2009**, *11*, 11276−11284.
(37) Akkerman, H. B.; Blom, P. W. M.; de Leeuw, D. M.; de Boer, B. Towards Molecular Electronics with Large-Area Molecular Junctions. *Nature* **2006**, *441*, 69−72.
(38) Van Hal, P. A.; Smits, E. C. P.; Geuns, T. C. T.; Akkerman, H. B.; De Brito, B. C.; Perissinotto, S.; Lanzani, G.; Kronemeijer, A. J.; Geskin, V.; Cornil, J.; Blom, P. W. M.; De Boer, B.; De Leeuw, D. M.

Upscaling, Integration and Electrical Characterization of Molecular Junctions. *Nat. Nanotechnol.* **2008**, *3*, 749−754.
(39) Klauk, H.; Zschieschang, U.; Pflaum, J.; Halik, M. Ultralow-Power Organic Complementary Circuits. *Nature* **2007**, *445*, 745−748.
(40) Pimentel, G. C.; McClellan, A. L. *The Hydrogen Bond*; W. H. Freeman and Company: San Francisco, 1960.
(41) Socrates, G. *Infrared Characteristic Group Frequencies*, 2nd ed.; Wiley: New York, 1980.
(42) Deacon, G. B.; Phillips, R. J. Relationships Between the Carbon-Oxygen Stretching Frequencies of Carboxylato Complexes and the Type of Carboxylate Coordination. *Coord. Chem. Rev.* **1980**, *33*, 227−250.
(43) Anselmi, C.; Mosconi, E.; Pastore, M.; Ronca, E.; De Angelis, F. Adsorption of Organic Dyes on TiO_2 Surfaces in Dye-Sensitized Solar Cells: Interplay of Theory and Experiment. *Phys. Chem. Chem. Phys.* **2012**, *14*, 15963−15974.
(44) Howie, W. H.; Claeyssens, F.; Miura, H.; Peter, L. M. Characterization of Solid-State Dye-Sensitized Solar Cells Utilizing High Absorption Coefficient Metal-Free Organic Dyes. *J. Am. Chem. Soc.* **2008**, *130*, 1367−1375.
(45) Gloos, K.; Koppinen, P. J.; Pekola, J. P. Properties of Native Ultrathin Aluminium Oxide Tunnel Barriers. *J. Phys.: Condens. Matter* **2003**, *15*, 1733−1746.
(46) Van de Ruit, K.; Katsouras, I.; Bollen, D.; van Mol, T.; Janssen, R. A. J.; de Leeuw, D. M.; Kemerink, M. The Curious Out-of-Plane Conductivity of PEDOT:PSS. *Adv. Funct. Mater.* **2013**, *23*, 5787.